Optimal contact geometry for CdZnTe pixel detectors

Aleksey E. Bolotnikov, Steven E. Boggs, C. M. Hubert Chen, Walter R. Cook, Fiona A. Harrison, et al.

Aleksey E. Bolotnikov, Steven E. Boggs, C. M. Hubert Chen, Walter R. Cook, Fiona A. Harrison, Steven M. Schindler, "Optimal contact geometry for CdZnTe pixel detectors," Proc. SPIE 4141, Hard X-Ray, Gamma-Ray, and Neutron Detector Physics II, (21 November 2000); doi: 10.1117/12.407587

SPIE.

Event: International Symposium on Optical Science and Technology, 2000, San Diego, CA, United States

Investigation of optimal contact geometries for CdZnTe pixel detectors

Aleksey E. Bolotnikov*, Steven E. Boggs, C. M. Hubert Chen, Walter R. Cook, Fiona A. Harrison, and Stephen M. Schindler

California Institute of Technology, Pasadena, CA 91125

ABSTRACT

We are developing CdZnTe pixel detectors for use as focal plane sensors in astronomical hard X-ray telescopes. To optimize the spectral response and imaging performance, we are investigating the effect of contact geometry on charge collection. Specifically, we have studied contact designs with orthogonal thin strips placed between pixel contacts. We apply a negative bias on the grid with respect to the pixel potential to force charge to drift toward the contacts. The grid bias is selected to be just sufficient to avoid charge collection on the grid, while increasing the transverse electric field on the surface between contacts. In contrast to focusing electrodes designed to force field lines to terminate on the pixel contact, our approach allows us to overcome the effects of charge loss between the pixels without significant increase of the leakage current, improving the overall energy resolution of the detector. In this paper we describe the performance of a CdZnTe pixel detector containing a grid electrode, bonded to a custom low-noise VLSI readout. We discuss the advantages of this type of detector for high spectral resolution applications.

Keywords: X-ray astrophysics – CdZnTe pixel detectors

1. INTRODUCTION

Charge loss between contacts of traditional pixel detectors (those with the anode segmented into individual contacts held at the same potential) has limited the spectral performance of these devices when events occurring between pixels are included in the pulse-height distribution. In developing a focal plane detector for the balloon-borne High-Energy Focusing Telescope (HEFT) [1,2], we have evaluated a contact geometry designed to improve the charge collection efficiency in CdZnTe (CZT) pixel sensors. In our detectors, we include very thin strips between the rectangular pixel contacts, held at a potential intermediate between cathode and anode, the main purpose of which is to increase the electric field on the surface between pixel contacts. Although the idea of using additional electrodes (usually called focusing or steering electrodes) is not new (it has been employed in numerous types of gaseous and semiconductor detectors [3,4]), the purpose of the grid in our application is not to focus the field lines onto the contacts, but rather to supply sufficient transverse electric field on the surface to redirect field lines to the contacts. This minimizes additional leakage current introduced by the intermediate electrode, resulting in improved spectral resolution.

If an incident photon is absorbed over the pixel contact of a conventional CdZnTe detector, and all the electrons from the cloud are collected by a single contact (except those trapped in the bulk), the pulse will be detected on a single pixel. If, however, the interaction takes place over pixel boundaries, or the electron cloud expands (due to diffusion) outside the perimeter of the contact, the total charge produced will be shared between two or more pixels. We call this a charge-split event. In the latter case the signals from adjacent pixels should be added together to recover the total produced charge. This procedure increases the electronic noise component of the total energy proportionally to the electronic noise of a single pixel multiplied by the square root of the total number of added signals. If the electronic noise is small, this will not significantly degrade the overall energy resolution. However, if the charge is not totally collected–i.e. some fraction of charge is trapped near the surface–this can significantly degrade resolution, and leads to low energy tails in the pulse-height spectra. An easy way to see this effect is to plot the correlation between the pulse heights, A_1 and A_2, from two adjacent pixels for the events when points of interactions lie between these two pixels. If no charge loss is assumed, then $A_1+A_2=E$, where E is the photon energy, and, consequently, the dots in the plot corresponding to the events with the same energy E should lie on a straight

* Correspondence: Email: bolotnik@srl.caltech.edu; Telephone: 626-395-4488

Hard X-Ray, Gamma-Ray, and Neutron Detector Physics II, Ralph B. James, Richard C. Schirato, Editors, Proceedings of SPIE Vol. 4141 (2000) © 2000 SPIE. · 0277-786X/00/$15.00

line at 45 degrees to the vertical and horizontal axes. In the opposite case, the curvature of the line would be the signature of the charge loss between the pixel contacts (Fig. 4).

In our previous studies [5-8], we found that charge is lost near the surface between the pixel contacts of CZT detectors. We attribute this effect to the high conductivity of the CZT surface, which makes the electric field originating near the top at the boundary between pixels terminate on the surface between contacts. As a result, a large fraction of the electrons driven to the surface by the electric field will be lost because of the high trapping rate at the CZT surface. In the case of the conventional contact geometry, the field lines approach the surface between the contact nearly perpendicularly, then turn 90 degrees and enter a very thin layer at the surface. It is clear that in the middle of the gap where the field lines turn in opposite directions, the transverse component of field is very small, resulting in low charge collection efficiency from this area. For large contact gaps, the charge produced over pixel boundaries could be entirely lost, leading to dead areas between the pixel contacts [5].

Although the nature of the CZT surface conductance is not fully understood, its influence on the performance of multi-electrode detectors is important [5,9,10]. Due to the lack of experimental information, we assume that the surface conductance results from high-density surface states located within the energy gap, as demonstrated for Si, Ge, GaAs and others semiconductors. Two types of conductance can contribute to the measured surface current of semiconductors. One type is conduction in a space charge layer existing in the sub-surface region in many semiconductors. This layer is formed as a result of the energy band bending near the surface, and its type (inversion, depletion, or accumulation) depends on the surface potential and bulk properties of the semiconductor [11]. As an example, the space charge layer is formed inside a metal-insulator-semiconductor (MIS) structure, and controlled by the varying potential of a gate electrode (gate-controlled space charge layer) [12]. Theoretically, in high-resistivity semi-insulating (SI) material such as CZT, the inversion or accumulation layer could also exist between contacts separated even by un-gated surface areas. However, when a bias voltage is applied, the layer will be rapidly depleted. The second type is the surface state band conductance. Again, due to the lack of data, we refer to other semiconductors where similar effects were observed and studied. For example, the conductance of the Si surface was studied by Hasegawa et al [13], and was attributed to the two-dimensional metallic-like states localized on the Si surface. A similar idea was proposed by Jin et al [14] to explain the effects related to the surface conductance of GaAs devices. According to the latter work, thermally emitted electrons occupy the surface state band located close to the conduction band edge. The electrons in this band are confined within the thin layer near the surface by the potential barrier whose value is the difference between the conduction band edge and the surface state band. The electrons are free to move along the surface but have to overcome the potential barrier in order to penetrate inside.

In order to prevent field lines from intersecting the surface one has to increase the surface resistivity. This can be achieved by using chemical surface treatment that reduces the density of the surface states. For example, it is well known that oxygen exposure decreases the surface conductance of Si and Ge, and it was recently proved that surface oxidation significantly increases the surface resistivity of CZT as well [10]. However, despite all these improvements, the surface conductivity remains still too high in comparison to the bulk conductivity of the depleted CZT sample. Furthermore, the electrons can still reach the surface as the result of a diffusion process.

To avoid charge loss between pixels, we investigated a conventional contact pattern with small gaps [7,8]. For each individual pixel of a 100 μm gap, 8x8 pixel detector, we obtained very good spectra with the source collimated within a pixel contact (typical FWHM for the 59.5 keV line was 670 eV at $-10\ ^{0}C$). However, even with such a small gap, we observed strong bending of the correlation curve for the charge-split events. As a result, the added signals from two adjacent pixels did not produce good pulse-height spectra, even though we employed a correction for the bending. Another solution to this problem, which we present here, is to place very thin negatively biased electrodes in the middle of the gaps to increase the electric field on the surface, and thus, to improve the charge collection efficiency. A similar approach to the contact pattern design was used by He et al [3]; however this important role of the grid and the optimal geometry of the grid were not discussed in this work.

2. EXPERIMENTAL SETUP

In the measurements described here, we used a CZT sensor bonded to a custom low-noise VLSI readout hybrid designed in our laboratory. The sensor consists of a 7.6x7.8x2 mm^3 CdZnTe crystal with an 8x8 array of platinum contacts on one side and a monolithic contact on the opposite, made by eV-Products, indium bump bonded to the 64 channel readout chip. A detailed description of the hybrid and electronics can be found in our previous publications [7,8]. The new contact pattern has 50-μm wide strips (that formed the grid) placed between pixel contacts, as shown in Fig. 1. The contacts are evenly spaced with a 650 by 680 μm pitch, and are arranged in four groups. Each group differs from the others by the size of the gaps between the strips and the contacts, which varies from group to group over the range of 100 to 250 μm with 50 μm strips. We

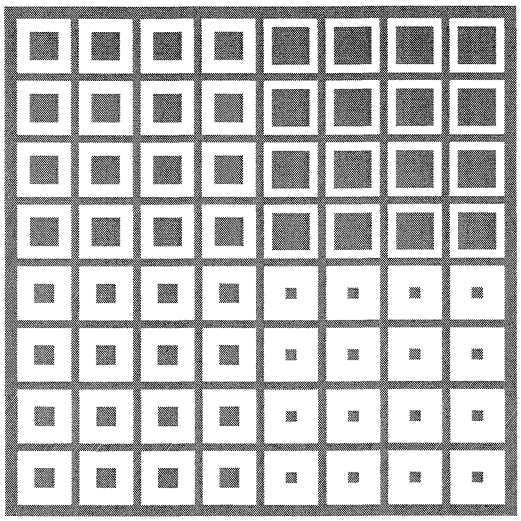

Figure 1. Pixel contact pattern with a grid.

mounted the hybrid and associated circuitry inside a temperature controlled chamber. A collimated ^{241}Am source could be precisely positioned over the detector using computer controlled stages. The full width of the beam at the detector cathode was 270 μm, diverging to a width of 350 μm at a depth of 1 mm. The collimated source was sealed in a steel container, which altered the low energy lines in the ^{241}Am spectrum.

We purchased several CZT detectors selected from the same slice, identically processed by eV-Products to fabricate the hybrids. We selected the two samples with the lowest total leakage current (measured at –300 V bias on the cathode) for processing, while we employed the rest for bulk and surface leakage current measurements. These were done using a probe stage with a GPIB controlled HP 3458A multimeter and an EDC 521 DC calibrator. We took special care to maintain steady state current condition during the measurements. After each voltage increase we wait for several minutes before taking 10 sequential measurements of current with 1 min intervals. This allows us to verify that equilibrium has been achieved before taking data. We made all measurements at room temperature, 26 (+/-1) ^{0}C, in air.

3. RESULTS AND DISCUSSION

3.1. Leakage current measurements

The pixel contact enclosed inside the guard ring (grid) offers a very suitable geometry for measuring bulk and surface leakage currents. Figure 2 shows an *I-V* curve of the surface leakage current measured through a pixel contact when a voltage is applied on the grid while the cathode is at zero potential. In order to prove that the measured current is indeed the surface leakage current, we measured the current between the contacts of two adjacent pixels for the two cases: the grid grounded and the grid floating. When the grid was grounded the measured current dropped by two orders of magnitude in comparison to the floating grid case. As seen in Fig. 2, between –10 and +10 V, the current follows a linear law, which indicates the metal-like surface state conductance on CZT. At high voltages, the current dependence gradually changes to a cube-law, an indication of double carrier injection from the contacts at high fields [9]. We observed similar behavior for all pixels. However, the current magnitude (measured at the same voltage) for pixels with the same gap size varies from pixel to pixel. The initial currents varied by more than an order of magnitude. Over two weeks time, the pixels with high surface current gradually improved, and current variations became less than 50%. The observed "forming" effect, i.e. an increase in the surface resistivity in the gap between the contact and the grid after it is kept biased for one-two weeks, can be explained by voltage stimulated surface oxidation that reduces the density of the surface states. Several groups have observed that an oxide layer formed on CZT reduces the surface leakage current [10,11]. The saturated surface resistivities evaluated from *I-V*

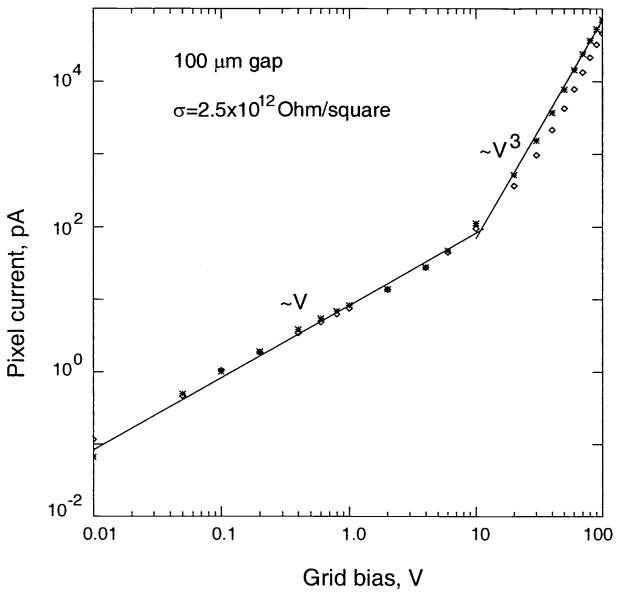

Figure 2. Surface leakage current measured between the grid and pixel contact; the cathode is at zero potential.

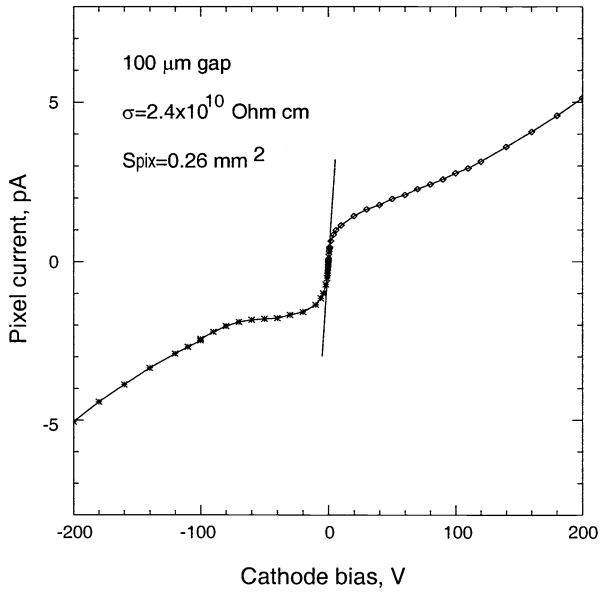

Figure 3. Bulk leakage current measured through the 100 μm gap pixel contact; the grid is at zero potential.

curves measured between -10 and +10 V for the 100 μm gap pixels were between (2.0-2.5)x10^{12} Ohm/square. These values are close to those reported in Ref [10].

In contrast to the surface leakage, we observed the measured bulk leakage current to be more stable. Figure 3 shows a typical bulk *I-V* curve measured through a pixel contact when a voltage is applied on the cathode, with the grid at ground potential. The dependence is clearly not linear. This suggests that Schottky-type barriers form under the Pt contacts. If the CZT detector is a simple metal-semiconductor-metal (MSM) structure with two barrier contacts, according to Sze et al [16], Ohmic current would be expected at low voltages, and thermionic emission current (over the potential barrier at the reverse-biased contact) would be observed at high voltages. This is clearly not observed, and could indicate the influence of deep levels existing in CZT. Since at low biases (<0.1 V) the resistance of the contact is small (typically 10^7-10^8 Ohm), we can evaluate the bulk resistivity by calculating the reciprocal derivative of the current at zero bias. We find it to be within +/-20% of the 3x10^{10} Ohm cm specified by eV products.

3.2. Pulse height spectrum measurements with the collimated source

In order to check the hybrid readout chip and to confirm our previous results, we measured pulse height spectra with the collimated ^{241}Am source positioned over the center of one pixel. Among the four groups of pixels, we obtain the best energy resolution for 100- and 150-μm gap pixels. With the *off-chip* shaping amplifier (1 μs shaping time) and a temperature of –10 ^{0}C, we obtain a FWHM of the 59.5 keV line of 570 and 580 eV, respectively. The cathode voltage was -350 V, and -15 and -25 V were applied on the grid for 100 and 150 μm gaps, respectively. (The FWHM of the test pulse peaks were 260 and 280 eV). These results were slightly better than our previous measurements with conventional pixel detectors [5]. This is primarily due to the smaller pixel capacitance of the "gridded" detector. For 200 and 250 μm gaps, the resolution was not as good as for smaller gaps. This is because of the larger electronic noise, due to the higher required grid voltage and consequently higher surface leakage current. Based on these data, we calculate the effective Fano-factor, which decreases from 0.18 to 0.14 as the cathode voltage increases from 250 up to 400 V. These relatively large numbers indicate some field-dependent effects that degrade the energy resolution. With the *on-chip* shaping amplifier, we measured the FWHM of 0.8-1.1 keV (depending on the grid bias) for the 59.5 keV line and 600-800 eV electronic noise at room temperature (26 ^{0}C). Again, these are slightly better results than those previously obtained with "ungridded" detectors.

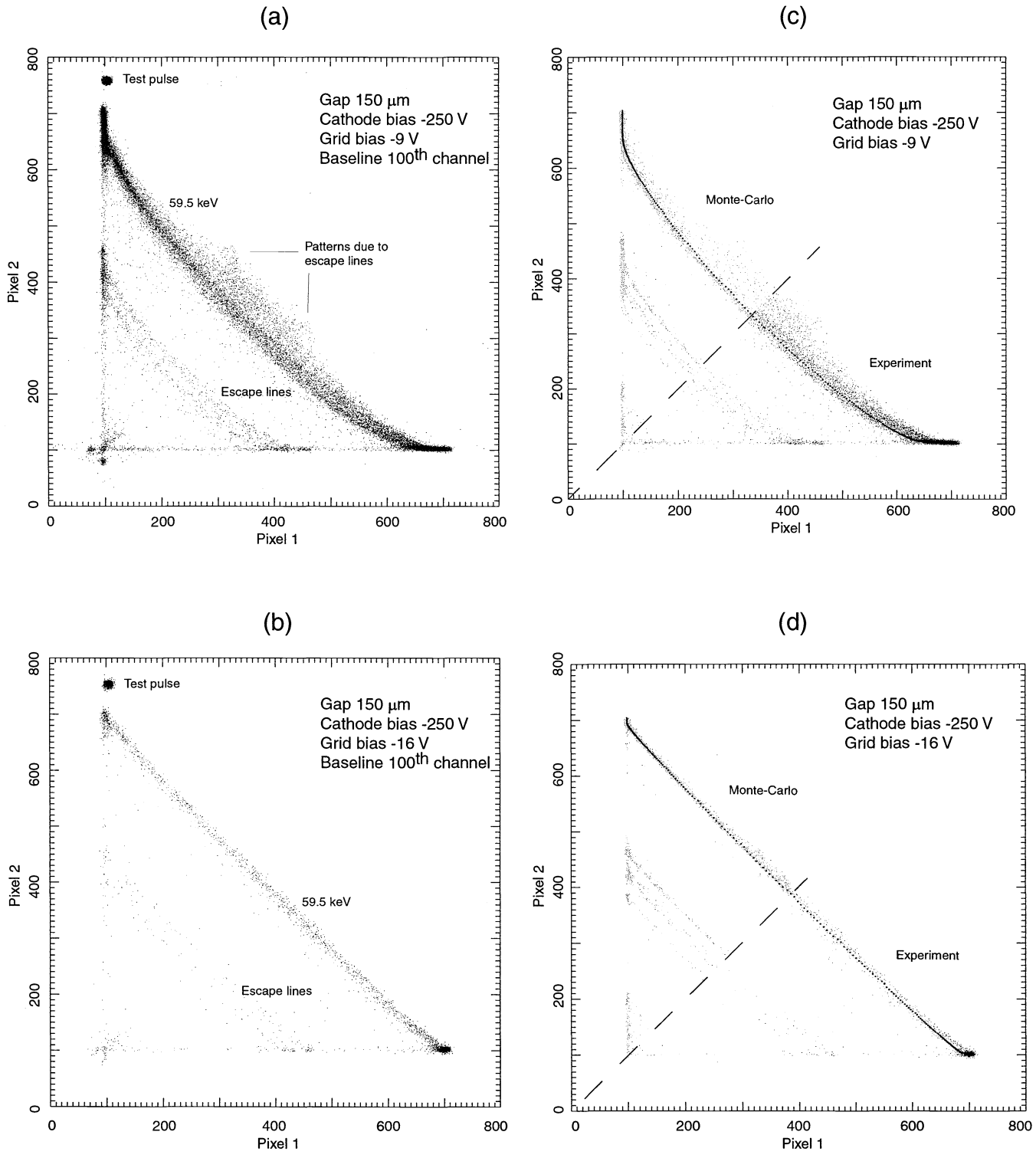

Figure 4. Correlation curves measured for 150 μm gap pixels with -9 V (a) and -16 V (b) on the grid. The results of the fitting procedure (dark dotted line) and Monte-Carlo modeling (upper parts of the curves) are shown in (c) and (d).

3.3. Correlation curve measurements

We studied the effect of the grid on the charge sharing between two adjacent pixels with a collimated ^{241}Am source positioned over the boundary between two pixels. We measured the pulse heights from the two adjacent pixels, and plotted the correlation between two pulse-heights for two cases: a) one or b) both pixels triggered. For these measurements we set the electronic threshold as low as possible. As an example, Fig. 4(a) and 4(b) show two representative correlation curves measured for 150 μm gap pixels at low (-9 V) and high (-16 V) biases on the grid, respectively. In these plots, each X-ray event is represented by a single dot. As explained in the introduction, for the events produced by X-rays with the same energy, the dots are concentrated along the correlation curve at 45 degrees to the vertical and horizontal axes, with the curvature being due to signal loss. The upper line corresponds to the 59.5 keV X-rays. Other lines due to the CZT escape peaks are apparent on the plots. The dots concentrated around the vertical and horizontal baselines are due to events where charge is shared with one of the other adjacent pixels (besides the two under consideration). One of the factors determining the width of the distribution in the direction perpendicular to the lines is the electronic noise, clearly seen as a wide cluster corresponding to the test pulse events. Several distinguishing features are evident on the low grid bias curve, some of which can also be seen on the high grid bias curve as well. These features are: drops (vertical and horizontal) near the ends of the correlation line, the line's curvature, and a broad distribution above the correlation curve near the center.

Schematically, the charge sharing process can be considered as follows. A charge produced by the incident photon near the cathode travels 2 mm in a nearly uniform field toward the anode. Due to strong diffusion, the original point-like charge distribution becomes broader, and can be described in the lateral direction near the anode surface by the Gaussian function. We calculate the sigma of the distribution (in the case of one-dimensional diffusion) to be 30 μm, taking the diffusion coefficient D, as 25 cm^2/s, electron mobility μ, as 960 cm^2/Vs [6], and assuming a 250 V bias on the cathode. Thus, 99.7% of the total charge is located within 180 μm (6 sigma)–the size comparable to the gap size between the contacts. In reality, the exact shape of the charge distribution is affected by field lines bending near the contacts, and thus, should be calculated by solving 3-D diffusion equations with the presence of the electric field. Nevertheless, as will be shown below, even a rough solution of this equation can explain the basic features of the correlation curves. Let us consider two adjacent pixels with the collimated source positioned over their boundary. If all charge arriving at the anode side lies within the contact's area of one pixel, the maximum signal will be read out from this pixel and just noise from the other. This corresponds to the topmost and rightmost points on the correlation curves (Fig. 4). If only a fraction of the charge arrives on one contact and the rest lands between the contact and grid, less signal will be read out from one pixel, and again only noise from the other. As a result, the correlation curve drops at the ends (the parts of the curve parallel to the axes). If the charge lands on both side of the grid strip that divides the two adjacent pixels, the signals from both pixels will be read out even though only one pixel is triggered. Since the size of the charge distribution is comparable to the gap size, in the first approximation, the percentage of charge trapped on the surface (or near the surface) is the same on both sides of the strip. Thus, one should expect to see the correlation curve as a *straight* line at 45 degrees to the vertical and horizontal axes shifted with respect to the topmost and rightmost points in axes directions by distances equal to the "drops". In reality, however, the line is curved primary because some fraction of charge is collected by the grid or trapped within the grid where the electric field is low. Since the strip is thin, for each charge-split event, it "removes" a very narrow "slice" from the gaussian-like distribution of the total charge arrived at the surface, i.e. the curvature of the lines in Fig. 4 reflects the gaussian distribution of the arrived charge. As seen in Fig. 4, there are additional dots patterns above the correlation curves which we attribute to the two-point interaction events caused by CZT escape photons.

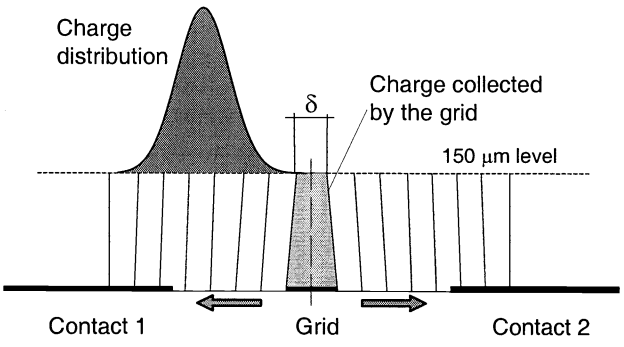

Figure 5. Approximation of the solution of the drift-diffusion equation near the pixel contacts.

In order to model these processes quantitatively, we use an approximate solution of the drift-diffusion equation for the 2-D case. We assume that the electrons originally produced near the cathode drift in a uniform field down to a level of 100 μm above the anode. At this level, the distribution of electrons, broadened by diffusion, is given by a gaussian with $\sigma=(2Dt)^{1/2}$, where t is the drifting time, D is the diffusion coefficient, $t=d/\mu E$, E is the electric

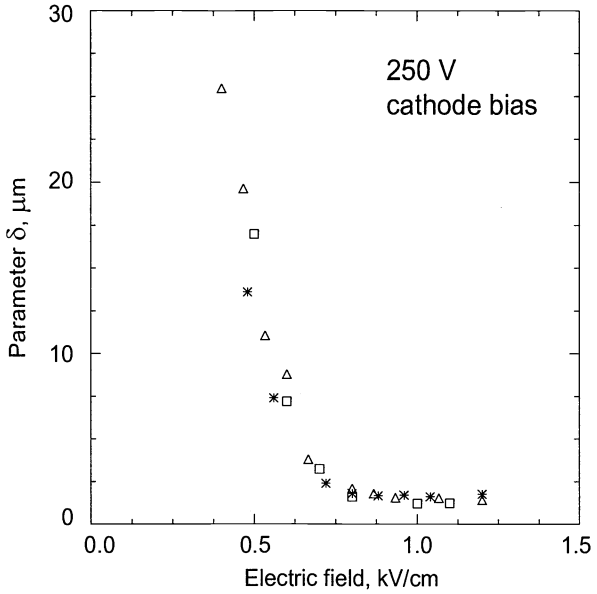

Figure 6. Parameter δ versus the electric field strength in a gap evaluated for 100, 150, and 250 μm pixel gaps.

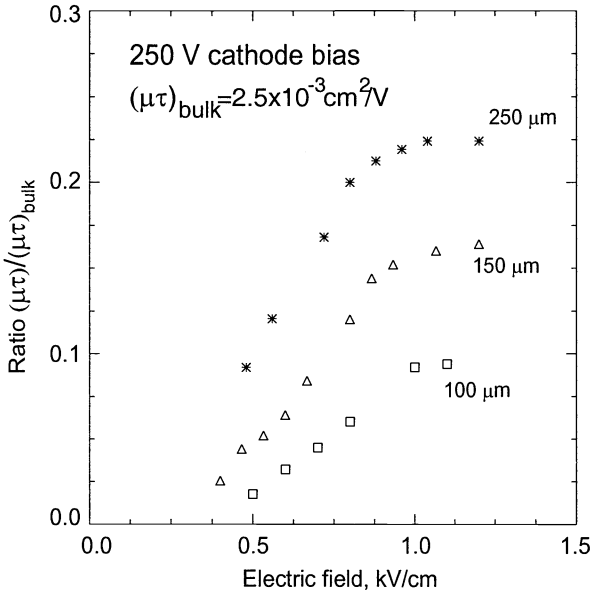

Figure 7. Parameter $\mu\tau$ versus the electric field strength in a gap evaluated for 100, 150, and 250 μm pixel gaps.

field strength, and d=2 mm. Below the 100 μm level the solution of the drift-diffusion equation can be constructed with the help of two adjustable parameters. Fig. 5 shows the one dimensional charge distribution along the line at a 100 μm level over two adjacent pixel. To find the charge distribution *G(x),* after it arrives to the surface we use the following transformation of the original gaussian. Let us assume, that the electrons arriving at the central region of the 100 μm line, δ, will travel further to the grid, while the electrons from outside this region will be evenly translated along straight lines toward the bare surface and contacts as shown in Fig. 5. The next step is to calculate the charge collected by the pixel contacts. We assume that all charge located within δ is lost, i.e. δ takes into account the charge loss on the grid strip (or in its vicinity where the field is low). To account for the charge loss on the surface and in the bulk, we introduce the second parameter - an *effective* $\mu\tau$-product. The fraction of charge loss after traveling a distance x along the surface is $1\text{-}exp(-xL/\mu\tau Ug)$, where Ug is the grid bias, and L is the grid to contact distance, and x is measured from the contact edge (if $x < 0$ all charge is collected on the contact). With these two parameters, finding a solution of the drift-diffusion equation in the area near the contacts becomes a simple geometrical problem.

Using this simple algorithm and having found the parameters δ and $\mu\tau$ from fitting the measured curves, we were able to reproduce very accurately all features on the correlation plots measured for different pixel gaps and grid biases. As an example, the least square fits of the experimental data are illustrated as dark dotted lines in Figs. 4 (c) and (d). In these plots, the upper half of the correlation curves (above the diagonal) are the results of Monte-Carlo simulation with the estimated δ and $\mu\tau$. As seen, the dot patterns over the correlation curve on both plots are correctly reproduced.

Figure 6 shows the dependence of the parameter δ evaluated for different pixel gaps versus electric field strength in the gap between the grid and the contact. The data, although obtained for different gaps, represents common behavior, and can be described with the same curve. The sharp change in the slope, as seen in the plot at around (0.75-0.8) kV/cm, corresponds to the change in the field line distribution when *all* field lines are pushed away from the grid and δ is reduced to its nearly saturated value (< 2 μm). The residual value of δ can be attributed to a small fraction (~1% of the total charge in the case of 150 μm gaps) of charge loss near the grid; a low field region exists near the grid strip and electrons can also diffuse to the grid.

The field dependence of the parameter $\mu\tau$ is shown in Fig. 7 for several pixel gaps. The changes is parameter $\mu\tau$ reflects in the changes of the real field line distribution and electron trapping rate at the surface with the grid bias. As seen, they also become saturated at (0.9-1) kV/cm, resulting in small residual drops of the correlation curve. At some point, while increasing the grid bias, the electric field in the gap becomes so strong that the charge loss at the surface is overcome entirely.

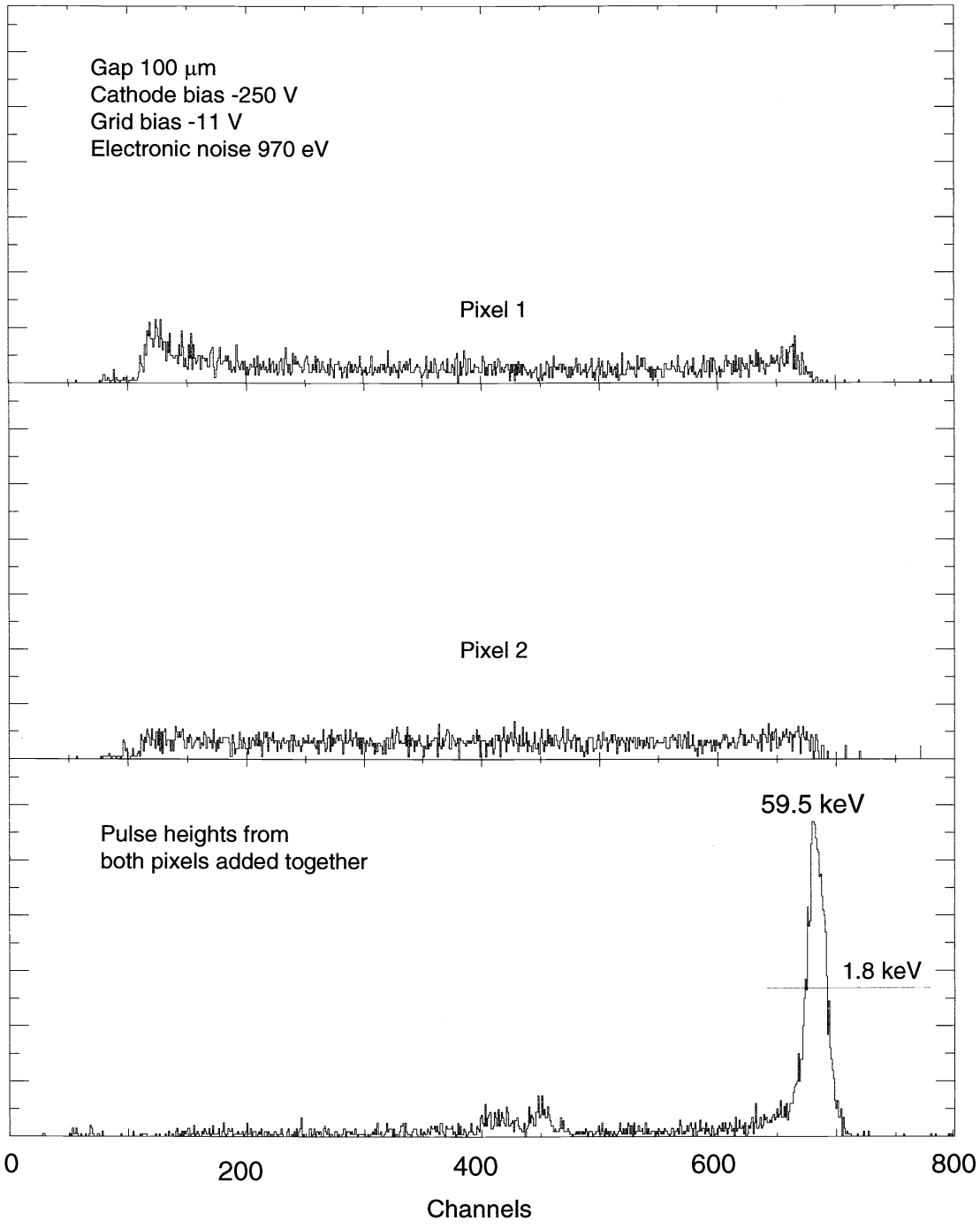

Figure 8. Pulse height spectra measured from two adjacent 100 μm gap pixels with the collimated source positioned over the pixel boundary. The spectrum at the bottom is obtained by adding the pulse heights from both pixels for each event.

However, charge loss in the bulk practically remains the same, causing the observed residual drops of the correlation curves (~1% of the total charge in the case of 150 μm gaps). The effect of the charge loss in the bulk can be reduced by applying a higher voltage on the cathode. Unfortunately, it will require a proportional increase of the grid voltage, which will result in the increase of the leakage current. In the previous section, we pointed out the large values of the Fano-factor which indicates some additional effects deteriorating the energy resolution. This could be the variation of charge loss in the bulk due to differences in the path lengths (or drifting times) which electrons travel from the original point to the pixel contact.

The two residual effects discussed above limit the energy resolution when signals from two adjacent pixels are added together. The correction applied by taking into account the shape of the correlation curve did not work because of the broadening of the correlation curve caused by the escape photons. This is illustrated in Fig. 8, which shows two pulse-height spectra, (a) and (b), collected from two adjacent 100 μm gap pixels with the collimated source positioned over the pixel boundary (both pixels are triggered). The third spectrum, (c), is obtained by adding the pulse heights from the pixels for each event. The cathode and grid biases were –250 V and –11 V, respectively. The FWHM of the 59.5 keV line estimated from the "added" spectrum was 1.8 keV, which exceeds the width that would be expected if only the contribution of the electronic noise (970 eV measured for a single pixel at 11 V on the grid) were taken into account. The true solution of the problems can be achieved by making the grid thinner and the gap between the grid and contacts smaller. The thinner grid also means that a smaller voltage is required to bend field lines away from the grid, and consequently smaller level of leakage current is expected. We are currently fabricating a new CZT-VLSI hybrid which will have a nearly optimal contact pattern with 25 μm grid strips, 50 μm gaps, and 500 μm pixes.

The above approach uses a simplified solution of the drift-diffusion equation, although good agreement with experimental data was obtained with the help of two adjustable parameters. Despite its simplicity it allowed us to understand the physical process governing the charge sharing in the CZT pixel detector with the grid. We are currently developing a comprehensive model, which accounts for the realistic 3-D field and electron diffusion inside a CZT detector with the minimum number of adjustable parameters.

4. CONCLUSIONS

We have tested a contact geometry incorporating thin orthogonal electrodes between the pixel contacts. This grid, biased up to 15-20 V, allows us to significantly increase the field on the CZT surface, and to entirely overcome the charge loss *on the surface* between contacts. For all contact patterns we tested, we could operate at a grid voltage at which the degradation of the resolution resulting from incomplete charge collection is negligible. The two dominant effects we were able to minimize are: 1) charge collection differences resulting from interaction depth variations, and 2) charge being collected on the grid rather than the contact. For the pattern with the smallest (100 μm) gap, the residual drop of the correlation curves is minimal. However, the contribution of both effects (currently on the ~1% level for a 150 μm gap) can be reduced well below the electronic noise level by reducing the size of the gap and making the grid thinner. Our modeling shows that for 50 μm gaps, a 25 μm wide grid, and a 500x500 μm pixel size, the contribution of these effects should be less than 0.2%.

ACKNOWLEDGMENTS

The authors wish to thank B. Kecman, J.A. Burnham and B. Matthews from CIT, and M. Fitzsimmons from JPL for helping to fabricate CZT detectors.

REFERENCES

1. P. H. Mao, F. A. Harrison, Y. Y. Platonov, D. Broadway, B. DeGroot, F.E. Christensen, W.W. Craig, and C.J. Hailey, "Development of grazing incidence multilayer mirrors for hard X-ray focusing telescopes", *Proc. of SPIE,* 3114, 1997.
2. W.W.Craig, F.E. Christensen, T. Decker, C.J. Hailey, F.A. Harrison, R.M. Hill, M. Jimenez-Garate, P. Mao, S. Schindler, *SPIE Proc.* 3445, pp. 112-120, *EUV, X-Ray, and Gamma-Ray Instrumentation for Astronomy IX*, 1998.
3. Z. He, W. Li, G.F. Knoll, D.K. Wehe, J. Berry, C.M. Stahle, Nucl. Instr. and Meth., A 422, pp.173-178, 1999.
4. M. Mayer, L.A. Hamel, O. Tousignant, J.R. Macri, J.M. Ryan, M.L. McConnell, V.T. Jordanov, J.F. Butler, C.L. Lingren, Nucl. Instr. and Meth. A 422, pp.190-19, 1999.

5. A. E. Bolotnikov, W. R. Cook, F. A. Harrison, A-S. Wong, S. M. Schindler, A. C. Eichelberger, Nucl. Instr. and Meth. A 432, pp.326-331, 1999.
6. A. E. Bolotnikov, S. E. Boggs, W. R. Cook, F. A. Harrison, S. M. Schindler, *Proc. of* SPIE, 3769, pp.52-58, 1999.
7. W.R. Cook, S.E. Boggs, A.E. Bolotnikov, J.A. Burnham, F.A. Harrison, B. Kecman, B. Matthews, S.M. Schindler and M.J. Fitzsimmons, "First Test Results from a High Resolution CdZnTe Pixel Detector with VLSI Readout", *Proc. of SPIE*, 3769, pp.92-96, 1999.
8. A. E. Bolotnikov, S. E. Boggs, W. R. Cook, F. A. Harrison, S. M. Schindler, accepted for publication in Nucl. Instr. and Meth. A, 1999.
9. Albert Rose, J. Appl. Phys. 35, pp.2664-2678, 1964.
10. M.J. Mescher, T.E. Schlesinger, J.E. Toney, B.A. Brunett, and R.B. James, Journal of Electronic Materials, 28, p. 700, 1999.
11. T.H. Pretty, M.A. Hoffbauer, J.A. Rennie, S. Cook, J.C. Gregory, M.A. George, P.N. Luke, M. Amman, S.A. Soldner, J.R. Earnhart, Nucl. Instr. and Meth. A 422, pp.179-184, 1999.
12. C.G.B. Garrett and W.H. Brattain, Phys. Rev. 99, pp. 376-387, 1955.
13. A.Y.C. Yu and E.H. Snow, J. Appl. Phys. 39, pp. 3008-3016, 1968.
14. Y. Hasegawa, I-W. Lyo, and P Avouris, Surface Science 357-358, p. 32, 1996.
15. G. Jin and B. K. Jones, J. Appl. Phys. 80, pp. 6340-6348, 1996.
16. S.M.Sze, D.J. Coleman, and A. Loya, Solid-State Electron. 14, p. 1209, 1971.